

# Turing patterns on networks

Hiroya Nakao<sup>1,2</sup> and Alexander S. Mikhailov<sup>2</sup>

<sup>1</sup>*Department of Physics, Kyoto University, Kyoto 606-8502, Japan and*

<sup>2</sup>*Abteilung Physikalische Chemie, Fritz-Haber-Institut der Max-Planck-Gesellschaft, Faradayweg 4-6, 14195 Berlin, Germany*

(Dated: July 8, 2008)

Turing patterns formed by activator-inhibitor systems on networks are considered. The linear stability analysis shows that the Turing instability generally occurs when the inhibitor diffuses sufficiently faster than the activator. Numerical simulations, using a prey-predator model on a scale-free random network, demonstrate that the final, asymptotically reached Turing patterns can be largely different from the critical modes at the onset of instability, and multistability and hysteresis are typically observed. An approximate mean-field theory of nonlinear Turing patterns on the networks is constructed.

PACS numbers: 82.40.Ck, 89.75.Fb, 87.23.Cc

Turing instability in activator-inhibitor systems is one of the most important classical concepts of nonequilibrium pattern formation [1], with diffusion destabilizing a uniform stationary state of the system and leading to formation of stationary spatial patterns. Turing patterns in ordinary continuous media have been extensively investigated in theoretical [2] and experimental [3, 4] studies. Their properties have also been studied for spatially heterogeneous systems [5] and in the presence of fractional diffusion [6].

In this Letter, we analyze Turing patterns exhibited by activator-inhibitor systems on networks. In such systems, the nodes are populated by activator and inhibitor species which are diffusively transported over the edges that form a network. As examples, multicellular systems [7], networks of coupled chemical reactors [8], and transportation networks that facilitate spreading of animals or insects [9, 10] can be mentioned. If several species are present, their mobilities on a network may significantly differ, and a situation is possible where the inhibitor species is much more easily transported over a network than the activator. Previously, it has been shown by linear stability analysis that the uniform stationary state in such networks can be unstable [7, 8]. However, detailed numerical and analytical investigations have so far been performed only for lattices [7] and for small network systems [8].

Here, we provide a complete linear stability analysis valid for any activator-inhibitor system and perform a detailed numerical study of Turing patterns in the Mimura-Murray model of interacting prey-predator populations [11]. Our numerical results reveal that the actual nonlinear behavior of network-based activator-inhibitor systems may show significant differences from the predictions of the linear stability analysis, with coexistence of many different structures and hysteresis being typically observed. As we further show, the properties of network Turing patterns can often be well understood in the framework of a mean-field approximation.

Activator-inhibitor systems on networks are described

by equations

$$\begin{aligned}\dot{U}_i(t) &= f(U_i, V_i) + \epsilon(\nabla^2 U)_i, \\ \dot{V}_i(t) &= g(U_i, V_i) + \sigma\epsilon(\nabla^2 V)_i,\end{aligned}\quad (1)$$

where  $U_i$  and  $V_i$  are concentrations of the activator and the inhibitor species on node  $i = 1, \dots, N$ , and functions  $f(U, V)$  and  $g(U, V)$  determine their local dynamics on a single node. In these equations,  $\nabla^2$  represents the diffusion (or Laplacian) operator on the network defined as  $(\nabla^2 U)_i = \sum_{j=1}^N A_{ij}(U_j - U_i)$  and  $(\nabla^2 V)_i = \sum_{j=1}^N A_{ij}(V_j - V_i)$ , where  $(A_{ij})$  is the adjacency matrix of the network. All nodes and edges in the network have the same properties. The parameter  $\epsilon$  is the diffusion constant of the activator, and  $\sigma$  is the ratio of the inhibitor diffusion constant to that of the activator. Note that the action of the network diffusion operator can also be expressed as  $(\nabla^2 U)_i = \sum_{j=1}^N L_{ij}U_j$  where  $(L_{ij})$  is the Laplacian matrix of the network, defined as  $L_{ij} = A_{ij} - k_i\delta_{ij}$  with  $k_i = \sum_{j=1}^N A_{ij}$  representing the degree of the node  $i$ .

In absence of diffusion ( $\epsilon = 0$ ), each network element has a linearly stable stationary state  $(U^{(0)}, V^{(0)})$ , which satisfies  $f(U^{(0)}, V^{(0)}) = 0$  and  $g(U^{(0)}, V^{(0)}) = 0$ . Since  $U$  is the activator and  $V$  is the inhibitor, we assume  $f_u = \partial f / \partial U|_{(U^{(0)}, V^{(0)})} > 0$ ,  $f_v = \partial f / \partial V|_{(U^{(0)}, V^{(0)})} < 0$ ,  $g_u = \partial g / \partial U|_{(U^{(0)}, V^{(0)})} > 0$ , and  $g_v = \partial g / \partial V|_{(U^{(0)}, V^{(0)})} < 0$ . When diffusion is turned on ( $\epsilon > 0$ ), the uniform solution  $(U_i, V_i) \equiv (U^{(0)}, V^{(0)})$  still satisfies Eqs. (1). However, this uniform solution may now become unstable due to the difference in diffusional mobilities of the activator and inhibitor species.

The linear stability analysis is naturally performed by using eigenvalues  $\Lambda^{(\alpha)}$  and eigenvectors  $\phi^{(\alpha)} = (\phi_1^{(\alpha)}, \dots, \phi_N^{(\alpha)})$  of the Laplacian matrix, satisfying  $(\nabla^2 \phi^{(\alpha)})_i = \sum_{j=1}^N L_{ij}\phi_j^{(\alpha)} = \Lambda^{(\alpha)}\phi_i^{(\alpha)}$  ( $\alpha = 1, \dots, N$ ). Since  $L_{ij}$  is a real symmetric matrix, all its eigenvalues are real, and its eigenvectors are mutually orthogonal. We sort indices  $\{\alpha\}$  in the decreasing order of the eigenvalues, so that  $0 = \Lambda^{(1)} > \Lambda^{(2)} > \dots > \Lambda^{(N)}$  holds.

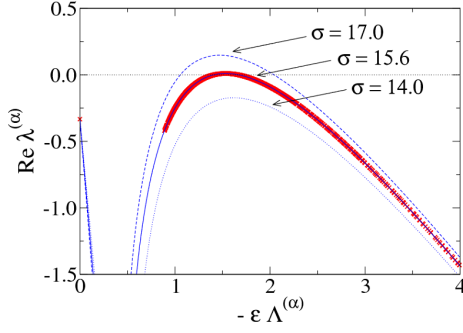


FIG. 1: (color online) Linear growth rates in the Mimura-Murray model on the scale-free network, with  $\text{Re } \lambda^{(\alpha)}$  plotted against  $-\epsilon \Lambda^{(\alpha)}$  for  $\epsilon = 0.12$  and three different values of the ratio  $\sigma$  of the diffusion constants. Crosses show actual discrete values of the growth rates for  $\sigma = 15.6$ .

Linearized equations describing evolution of small perturbations  $(u_i, v_i)$  to the uniform state  $(U^{(0)}, V^{(0)})$  are given by

$$\begin{aligned}\dot{u}_i(t) &= f_u u_i + f_v v_i + \epsilon (\nabla^2 u)_i, \\ \dot{v}_i(t) &= g_u u_i + g_v v_i + \sigma \epsilon (\nabla^2 v)_i.\end{aligned}\quad (2)$$

By expanding  $(u_i, v_i)$  over the Laplacian eigenvectors,  $(u_i, v_i) = \sum_{\alpha=1}^N (u^{(\alpha)}, v^{(\alpha)}) \exp[\lambda^{(\alpha)} t] \phi_i^{(\alpha)}$  where  $u^{(\alpha)}$  and  $v^{(\alpha)}$  are the expansion coefficients, Eqs. (2) are transformed into  $N$  independent linear equations for different modes  $(u^{(\alpha)}, v^{(\alpha)})$ . The linear growth rate  $\lambda^{(\alpha)}$  of the  $\alpha$ -th mode is determined from the characteristic equation  $\{\lambda^{(\alpha)} - f_u - \epsilon \Lambda^{(\alpha)}\} \{\lambda^{(\alpha)} - g_v - \sigma \epsilon \Lambda^{(\alpha)}\} - f_v g_u = 0$ , which yields

$$\lambda^{(\alpha)} = \left( f_u + g_v + (1 + \sigma) \epsilon \Lambda^{(\alpha)} \pm \sqrt{4 f_v g_u + (f_u - g_v + (1 - \sigma) \epsilon \Lambda^{(\alpha)})^2} \right) / 2. \quad (3)$$

When  $\text{Re } \lambda^{(\alpha)}$  is positive, the  $\alpha$ -th mode is unstable. The instability takes place when one of the modes begins to grow, namely, when  $\text{Re } \lambda^{(\alpha)} = 0$  for some  $\alpha = \alpha_0$  and  $\text{Re } \lambda^{(\alpha)} < 0$  for all other modes. For the Turing instability, the condition  $\text{Im } \lambda^{(\alpha)} = 0$  should also hold.

Graphically, all growth rates  $\lambda^{(\alpha)}$  lie on the curve  $\lambda = F(\Lambda)$ , which is determined by Eq. (3) (see Fig. 1). When the ratio  $\sigma$  of the diffusion constants is varied, this curve touches the horizontal axis at  $\sigma_c = (f_u g_v - 2 f_v g_u + 2 \sqrt{f_v g_u (f_v g_u - f_u g_v)}) / f_u^2$ , and some of the modes may therefore become unstable for  $\sigma > \sigma_c$ . For this to occur, the eigenvalues of the discrete Laplacian spectrum of the considered network must be actually present near the maximum of the curve. Therefore, the condition  $\sigma = \sigma_c$  provides only the lower bound for the Turing instability boundary.

Thus, the condition of the Turing instability on networks is similar to the respective condition for the continuous media. The role of plane waves is now played by Laplacian eigenvectors of the considered network, and, instead of wavenumbers, the respective Laplacian eigenvalues are important. Note that the above linear stability analysis is general; it holds for any activator-inhibitor model and for any network architecture. The critical mode always corresponds to a certain Laplacian eigenvector.

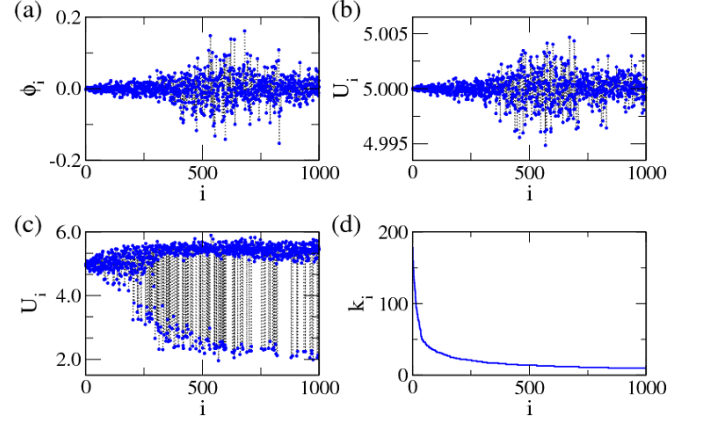


FIG. 2: (color online) (a) The critical mode (the Laplacian eigenvector with  $\alpha_0 = 422$ ), (b) the activator pattern at the early evolution stage ( $t = 200$ ), and (c) the stationary activator pattern at the late stage ( $t = 1500$ ). Nodes are ordered according to their degrees; with (d) showing the dependence of the degree on the node index.

To perform numerical investigations of nonlinear dynamics, a specific activator-inhibitor model is needed. For this purpose, we have chosen the Mimura-Murray model [11], which has been introduced to explain spatial nonuniformity of prey-predator populations in ecological systems. The chosen model is given by the equations  $f(U, V) = \{(35 + 16U - U^2)/9 - V\}U$  and  $g(U, V) = \{U - (1 + 2V/5)\}V$ , whose fixed point is  $(U^{(0)}, V^{(0)}) = (5, 10)$ . As an example of random networks, we take below the Barabási-Albert scale-free networks [13] of size  $N = 1000$ . They are generated by the preferential attachment algorithm, starting from 10 fully connected initial nodes and adding  $m = 10$  new connections at each iteration step, so that their mean degree is  $\langle k \rangle \simeq 2m = 20$ .

Figure 1 displays the real part of the linear growth rate  $\text{Re } \lambda^{(\alpha)}$  for three values of  $\sigma$  with  $\epsilon = 0.12$ . The growth rate can become positive for  $\sigma > \sigma_c = 15.5$ . The largest growth rate is reached at  $\alpha_0 = 422$  for  $\sigma = 15.6$ . Near  $\alpha = \alpha_0$ ,  $\text{Im } \lambda^{(\alpha)} = 0$  holds. In Fig. 2, we compare the critical mode ( $\alpha_0 = 422$ ) with two snapshots of the actual activator patterns at the early and late stages of the evolution, as yielded by numerical integration of Eqs. (1) with  $\epsilon = 0.12$  and  $\sigma = 15.6$ . Here and below, node in-

dices  $\{i\}$  are sorted in the decreasing order of their node degrees  $\{k_i\}$  so that  $k_1 \geq k_2 \geq \dots \geq k_N$  holds, which is useful in visualizing the Turing patterns exhibited by our system.

Starting from almost uniform initial conditions with tiny perturbations, exponential growth is observed at the early stage. The activator pattern at this stage, Fig. 2(b), is similar to the critical mode, Fig. 2(a), with the deviations due to contributions from a few neighboring modes that are already excited to some extent. Later on, however, strong nonlinear effects develop, and the final stationary pattern, Fig. 2(c), becomes very different from the one determined by the critical mode. Observing the nonlinear development (see Video [16]), we notice that some elements get progressively kicked off the main group near the destabilized uniform solution in this process. Eventually, in the asymptotic stationary state, all elements become separated into two groups. The correspondence between the indices and the degrees for the considered scale-free network is displayed in Fig. 2(d). The separation into two groups occurs only for the elements on the nodes with relatively small degrees (roughly  $i > 200$ ,  $k_i < 24$ ), while the elements on the nodes with high degrees ( $i < 200$ ,  $k_i > 24$ ) do not separate.

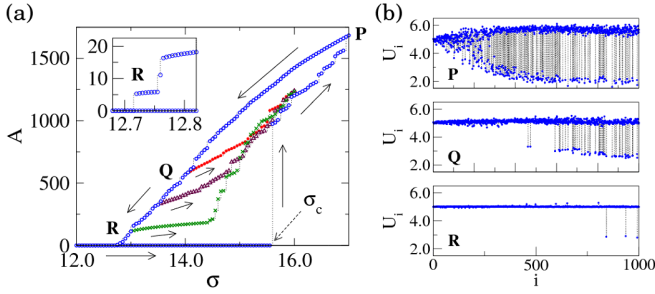


FIG. 3: (color online) (a) Amplitude  $A$  of the Turing pattern vs. the diffusion ratio  $\sigma$ ; variation direction of  $\sigma$  is indicated by arrows. (b) Stationary Turing patterns at parameter points  $P$  ( $\sigma = 17.0$ ),  $Q$  ( $\sigma = 13.5$ ), and  $R$  ( $\sigma = 12.8$ ). The inset in (a) shows the blowup near  $R$ .

The outcome of nonlinear evolution depends sensitively on initial conditions. Different Turing patterns are possible at the same parameter values and strong hysteresis effects have been observed. As an example, Fig. 3(a) shows how the amplitude of the stationary Turing pattern, defined as  $A = \sum_{i=1}^N \{(U_i - U^{(0)})^2 + (V_i - V^{(0)})^2\}$ , varies under gradual variation of the parameter  $\sigma$  in the upward or downward directions. Stationary patterns observed at points  $P$ ,  $Q$ , and  $R$  in Fig. 3(a) are presented in Fig. 3(b). As  $\sigma$  was increased starting from the uniform initial condition, the Turing instability took place at  $\sigma = \sigma_c$ , with the amplitude  $A$  suddenly jumping up to a high value that corresponds to the appearance of a kicked-off group. If  $\sigma$  was further increased, the amplitude  $A$  grew. Starting

to decrease  $\sigma$ , we did not however observe a drop down at  $\sigma = \sigma_c$ . Instead, a punctuated decrease in the amplitude  $A$ , which is characterized by many relatively small steps, was found. Reversing the direction of change of the parameter  $\sigma$  at different points, many coexisting solution branches could be identified. The characteristics of Turing patterns vary with their amplitudes. When  $A$  is close to zero (point  $R$  in Fig. 3), only a few kicked-off elements remain in the system. Because of the hysteresis, solutions with only a small number of destabilized elements can coexist with the linearly stable uniform state in this region, so that the localized Turing patterns are found for  $\sigma < \sigma_c$ .

The properties of the developed Turing patterns above the instability boundary ( $\sigma > \sigma_c$ ) can be relatively well understood by using the mean-field approximation, previously used for the analysis of epidemics spreading on networks [14] and for networks of phase oscillators [15]. We start by writing Eqs. (1) in the form

$$\begin{aligned}\dot{U}_i(t) &= f(U_i, V_i) + \epsilon(h_i^{(U)} - k_i U_i), \\ \dot{V}_i(t) &= g(U_i, V_i) + \sigma \epsilon(h_i^{(V)} - k_i V_i),\end{aligned}\quad (4)$$

where local fields felt by each element,  $h_i^{(U)} = \sum_{j=1}^N A_{ij} U_j$  and  $h_i^{(V)} = \sum_{j=1}^N A_{ij} V_j$ , are introduced. These local fields are further approximated as  $h_i^{(U)} \simeq k_i H^{(U)}$  and  $h_i^{(V)} \simeq k_i H^{(V)}$ , where *global mean fields* are defined by  $H^{(U)} = \sum_{j=1}^N w_j U_j$  and  $H^{(V)} = \sum_{j=1}^N w_j V_j$ . The weights  $w_j = k_j / (\sum_{j'=1}^N k_{j'}) = k_j / k_{total}$  take into account the difference in the contributions of different nodes to the global mean field, depending on their degrees (cf. [14, 15]). Thus, the local fields are taken to be proportional to the degree of a node, ignoring the details of its actual connections.

With this approximation, each element interacts only with the global mean fields, and its dynamics is described by

$$\begin{aligned}\dot{U}(t) &= f(U, V) + \beta(H^{(U)} - U), \\ \dot{V}(t) &= g(U, V) + \sigma \beta(H^{(V)} - V).\end{aligned}\quad (5)$$

We have dropped here the index  $i$ , since all elements obey the same dynamics, and introduced the parameter  $\beta = \epsilon k_i$ . If diffusion ratio  $\sigma$  is fixed and the global mean fields  $H^{(U)}$  and  $H^{(V)}$  are given, this parameter  $\beta$  plays the role of a bifurcation parameter that controls the dynamics of each element. Equations (5) have a single stable fixed point when  $\beta = 0$  (i.e.  $\epsilon = 0$ ), and, as  $\beta$  is increased, this system undergoes imperfect pitchfork bifurcations that give rise to two new stable fixed points.

We have computed stationary Turing patterns by numerical integration of Eqs. (1) and determined the respective global mean fields  $H^{(U)}$  and  $H^{(V)}$  at  $\sigma = 15.6$  and  $\sigma = 30$ . Substituting these computed global mean fields

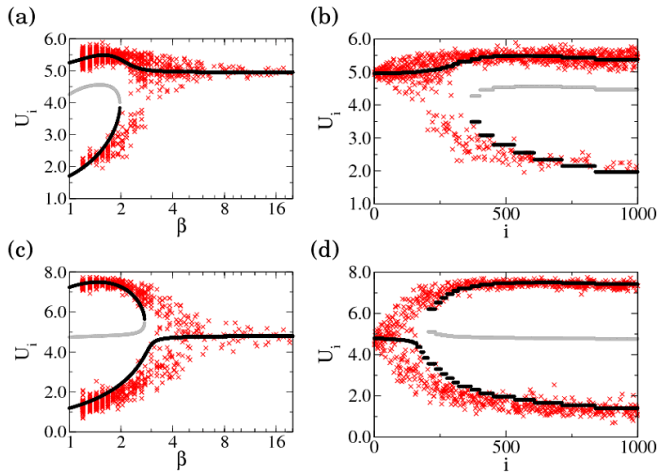


FIG. 4: (color online) Stationary Turing patterns compared with the bifurcation diagrams of a single element coupled to global mean fields. The parameters are  $\epsilon = 0.12$  and (a,b)  $\sigma = 15.6$ , (c,d)  $\sigma = 30$ . Black curves (dots) indicate stable branches, gray curves (dots) correspond to the unstable branch. Crosses show the computed Turing patterns. The global mean fields are  $(H^{(U)}, H^{(V)}) = (4.95, 9.97)$  for  $\sigma = 15.6$ , and  $(H^{(U)}, H^{(V)}) = (4.8, 9.9)$  for  $\sigma = 30$ .

into Eqs. (5), bifurcation diagrams for a single Mimura-Murray element have been obtained (solid curves in Fig. 4 (a,c)). These diagrams can be compared with the actual stationary Turing patterns. Each node  $i$  in the network is characterized by its degree  $k_i$ , so that it possesses a certain value of the bifurcation parameter,  $\beta = \epsilon k_i$ . Therefore, the Turing pattern can be projected onto these bifurcation diagrams, as shown by crosses in Fig. 4(a,c). We see a relatively good agreement between the stable branches and the data from the actual Turing patterns. Furthermore, we directly compare in Fig. 4(b,d) the computed Turing patterns with the mean-field predictions, based on Eqs. (5). We see that the Turing patterns are nicely fitted by the stable branches, though the scattering of numerical data gets enhanced near the branching points. In this way, the fully developed Turing patterns in our system are essentially explained by the bifurcation diagrams of a single element coupled to constant global mean fields, with the coupling strength determined by the degree of the respective network node.

Thus, we have constructed a general linear theory of Turing patterns in the activator-inhibitor systems on networks and have also performed numerical investigations of nonlinear pattern formation. The Turing instability takes place on any networks as the ratio of diffusion constants of the inhibitor and activator species is increased. The critical mode corresponds to a certain eigenvector of the Laplacian matrix, but the final Turing patterns may be very different from the critical mode; multistability of solutions and hysteresis are effects are typically

observed. Localized Turing patterns below the linear instability threshold have been found.

To understand this behavior, it should be taken into account that, while being relatively large ( $N = 1000$ ), the considered random networks had nonetheless only the small diameters of 4 and, moreover, each node in a network had 20 neighbors on the average. Therefore, diffusional mixing should be very strong in such activator-inhibitor systems, and behavior characteristic of small well-mixed spatial volumes can be expected; each element in a network may be viewed as interacting with some global mean fields. Indeed, separation of elements into two clusters has previously been reported for globally coupled activator-inhibitor systems under similar conditions [12]. The coupling to the global mean fields is however essentially heterogeneous in our case, because it is determined by the degrees of the respective network nodes which vary greatly. Although not included here, investigations have also been undertaken by us for the classical Brusselator model and for the Erdős-Rényi random networks, and similar results have been obtained. The constructed mean-field theory of nonlinear Turing pattern formation is applicable for various large random networks of small diameters and different activator-inhibitor systems.

Financial support of the Volkswagen Foundation (Germany) is gratefully acknowledged.

- 
- [1] A. M. Turing, Phil. Trans. R. Soc. B **237**, 37 (1952).
  - [2] D. Walgraef, *Spatio-Temporal Pattern Formation*, Springer, New York, 1996.
  - [3] V. Castets, E. Dulos, J. Boissonade, and P. De Kepper, Phys. Rev. Lett. **64**, 2953 (1990).
  - [4] Q. Ouyang and H. L. Swinney, Nature **352**, 610 (1991).
  - [5] K. M. Page, P. K. Maini, and N. A. M. Monk, Physica D **202**, 95 (2005).
  - [6] B. I. Henry, T. A. M. Langlands, and S. L. Wearne, Phys. Rev. E **72**, 026101 (2005).
  - [7] H. G. Othmer and L. E. Scriven, J. Theoret. Biol. **32**, 507 (1971); J. Theoret. Biol. **43**, 83 (1974).
  - [8] W. Horsthemke, K. Lam, and P. K. Moore, Phys. Lett. A **328**, 444 (2004); P. K. Moore and W. Horsthemke, Physica D **206**, 121 (2005).
  - [9] D. Urban and T. Keitt, Ecology **82**, 1205 (2001).
  - [10] M. A. Fortuna, C. Gómez-Rodríguez, and J. Bascompte, Proc. R. Soc. B **273**, 1429 (2006).
  - [11] M. Mimura and J. D. Murray, J. Theor. Biol. **75**, 249 (1978).
  - [12] T. Mizuguchi and M. Sano, Phys. Rev. Lett. **75**, 966 (1995).
  - [13] R. Albert and A. -L. Barabási, Rev. Mod. Phys. **74**, 47 (2002).
  - [14] R. Pastor-Satorras and A. Vespignani, Phys. Rev. Lett. **86**, 3200 (2001).
  - [15] T. Ichinomiya, Phys. Rev. E **70**, 026116 (2004).
  - [16] See EPAPS Document for a MPEG video showing evolution of the Turing pattern at  $\epsilon = 0.12$  and  $\sigma = 15.6$ .